공학석사 학위논문

Study on operating mechanism for all-solid-state Li-sulfur battery

전 고체 리튬 황 전지의 메커니즘 분석

2014년 2월

서울대학교 대학원

재 료 공 학 부

김 인 경

Study on operating mechanism for all-solid-state Li-sulfur battery

전 고체 리튬 황 전지의 메커니즘 분석

지도 교수 강 기 석

이 논문을 공학석사 학위논문으로 제출함

2014 년 2 월

서울대학교 대학원

재료공학부

김 인 경

김인경의 석사 학위논문을 인준함

2014 년 2 월

위 원 장 장 호 원 (인)

부위원장 남 기 태 (인)

위 원 강 기 석 (인)

Abstract

Study on operating mechanism for all-solid-state Li-sulfur battery

Inkyung Kim

Department of Material Science and Engineering

College of Engineering

The Graduate School

Seoul National University

Recently, sulfur is chosen as a cathode material for Li ion rechargeable battery (LIB) with its high theoretical capacity, environmental friendliness and low cost. However, shuttle mechanism (reduction in discharge capacity, overcharge) caused by dissolved lithium polysulfides is the main obstacle for practical use. In this thesis, solid electrolyte is used for Li-sulfur battery to eliminate the shuttle mechanism. Thio-LiSICON II analogue Li_2S-P_2S_5 solid electrolyte was adopted as a solid electrolyte with high lithium ionic conductivity, low temperature synthesizing process, and stable interface with Li metal. To begin with, construction of all-solid-state Li-sulfur battery was carried out to evaluate performance. Afterwards, Raman spectroscopy and XPS were used to find out intermediates and mechanism of all-solid-state Li-sulfur battery. During charging, Li_2S was oxidized to defective Li_2S and later on to short-chain lithium polysulfide and finally to sulfur. During discharging, reverse reaction was occurred. Examined defective Li_2S after 1^{st} charge might be correlated to irreversible capacity and poor cycle life. Solid electrolyte-Li_2S-carbon composite can be a solution to control interfaces among cell

components.

Keywords: all-solid-state, Li-sulfur battery, thio-LiSICON, defective Li_2S, polysulfide
Student Number: 2012-20583

Contents

List of Tables

List of Figures

Chapter 1. Introduction

Excessive consumption of limited fossil fuel triggers global warming and abnormal climate change. Concerning these environmental symptoms provokes intensive efforts to do research on renewable energy resources including solar energy, wind energy, geothermal energy, and ocean energy. Since renewable energy is time and space restricted resources, we need energy storage system for electric vehicles (EV) and hybrid electric vehicles (HEV) or smart grid system applications.

Li ion rechargeable battery (LIB) is one of the most promising candidates in terms of power density and volumetric and gravimetric energy density as shown in Fig.1.1 and Fig 1.2. However, there is a substantial gap between the performance of existing LIB technology and the battery requirements for future energy storage applications [3].

Recent researchers are interested in Li-sulfur battery among various LIBs. Li-sulfur battery has gravimetric energy density five times higher than that of conventional batteries as shown in Fig. 1.3 [4]. Though low equilibrium voltage of sulfur, high specific capacity induces high gravimetric energy density. Also, sulfur is non-toxic and low cost of sulfur. Table 1 compares electrochemical properties between conventional LIBs and Li-sulfur battery.

Despite those virtues of sulfur cathode, low practical specific energy and low cyclability restrict commercialization. It has been reported that dissolution of intermediate species and low conductivity of discharged and

charged products are reason for restricted electrochemical properties. Details of Li-sulfur battery mechanism will be explained in chapter 2.

In this thesis solid electrolyte is used to solve the dissolution problem of the Li-sulfur battery. Thio-Li ion super ionic conductor (LISICON) analogue phase was adopted as a solid electrolyte considering electrochemical stability and ionic conductivity. We also attempt to analysis the mechanism of thio-LISICON analogue for Li-sulfur battery. Details will be explained in chapter 3 and 4.

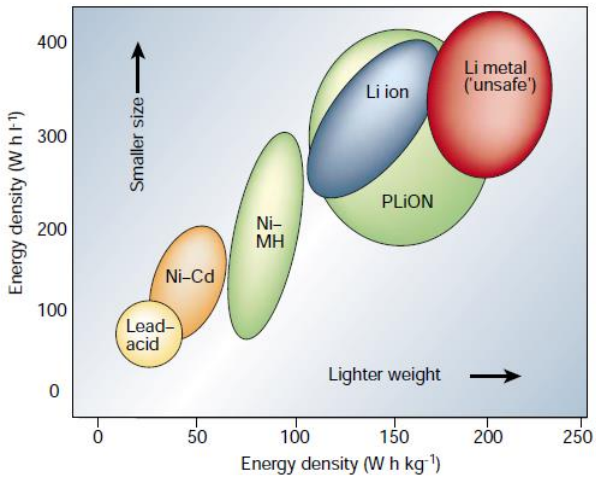

Fig.1.1 Gravimetric and volumetric energy density of energy storage systems [1]

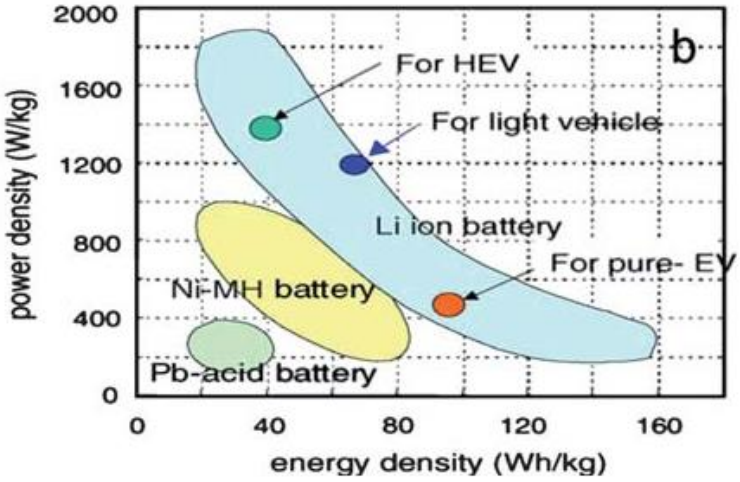

Fig.1.2 Ragone plot of energy storage systems [2]

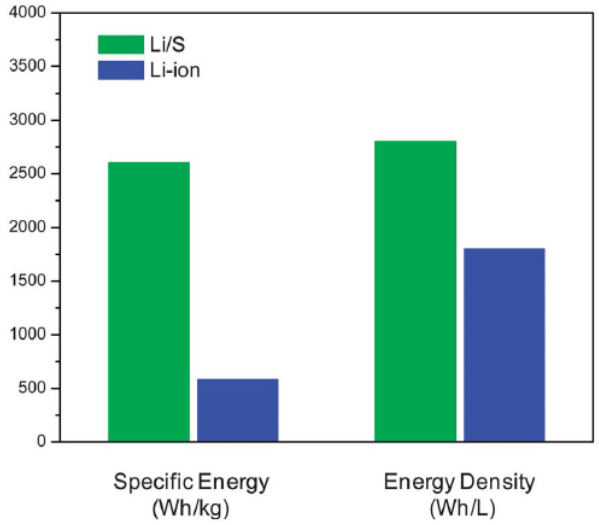

Fig. 1.3 Gravimetric and volumetric energy density of conventional and Li-sulfur battery

Characteristic	Lithium-ion cells	Lithium/sulfur cells
Cell voltage	3.4–4.0 V	2.15 V
Cathode specific capacity	140–200 mA h g^{-1}	1675 mA h g^{-1}
Theoretical specific energy	500–600 W h kg^{-1}	~2600 W h kg^{-1}
Practical (obtainable) specific energy	150–200 W h kg^{-1}	200–700 W h kg^{-1} (estimated)
Theoretical energy density	~1800 W h L^{-1}	~2800 W h L^{-1}
Cycle life (current status)	300–1000 deep cycles	<200 cycles

Table 1 Characteristics of conventional and Li-sulfur battery [4]

Chapter 2. Literature review

2.1 Li-sulfur battery

2.1.1 Mechanism of Li-sulfur battery

The first Li-sulfur battery was introduced in 1962 [4]. In the early stage of Li-sulfur battery research, electrochemical analysis and UV-vis absorption spectroscopy were used to elucidate discharge/charge mechanism [5, 6, 7]. Some results disagree with current researches. Due to the rapid consumption of lithium metal and poor cycle life [8, 9], interests on Li-sulfur batteries had decreased. Recently, interest in Li-sulfur battery is increasing as the powerful candidate for future energy storage system and it is essential to know exact electrochemical reaction mechanism for improving performance. Fig. 2.1 shows general discharge/charge profile of liquid state Li-sulfur battery. Some researchers refocused on elucidating Li-sulfur mechanism combined with structural analysis.

In 2003, structural analysis to Li-sulfur battery at the first time by S.-E. Cheon et al. [10]. The cathode was composed of sulfur (3-8 μm in particle size), super P, poly(butadiene-co-styrene) (58:28:13 by weight ratio). The electrolyte was 0.5 M $LiCF_3SO_3$ in tetra(ethylene glycol) dimethylether (TEGDME) and the anode was Li metal. Fig. 2.2 is a X-ray diffraction (XRD) profile of the discharged cathode (at 1.5 V) after completely washed with TEGDME. It shows that Li_2S is a discharged product of Li-sulfur battery. In

this paper, charged product was scarcely observed. After this paper ex-situ analysis using different electrolytes found Li_2S as a discharged product as the above [11, 12] but, no one confirmed sulfur as a charged product.

In 2012, in-situ analysis was firstly applied to Li-sulfur battery by J. Nelson et al. to figure out the mechanism without the addition of artifacts from post treatment [13]. The cathode was composed 70 wt% of heat treated sulfur (micrometer sized)-super P composite (1:1 by weight), 10 wt% super P, 20 wt% poly(vinylidene fluoride) (PVdF). The electrolyte was 1.0 M lithium bis(tri fluoro methane sulfonyl)imide (LiTFSI) in 1,3-dioxolane (DOL) and 1,2-dimethoxyethane (DME) (1:1 by volume) and the anode was Li metal. Though ex-situ XRD profile as shown in Fig 2.3 confirmed Li_2S peaks, no crystalline Li_2S peaks were found by in-situ XRD profile as shown in Fig 2.4. We can speculate amorphous Li_2S was formed after discharge from the electrochemical properties and ex-situ XRD profile. Reordered crystalline α-sulfur was confirmed as shown in Fig 2.4. However, detection of crystalline sulfur was affected by cathode preparation method.

In 2013, the research regarding in-situ XRD was which published by S. Walus et al. shows quite distinct result from previous reports [14]. The cathode was composed of sulfur, super P, PVdF (80:10:10 by weight ratio). The electrolyte was 1M LiTFSI in TEGDME and DOL (1:1 by volume). As shown in Fig 2.5, solid sulfur was completely dissolved out after 1^{st} discharge plateau and crystalline Li_2S was detected at a 2^{nd} discharge plateau. β–sulfur was firstly noticed as a charged product.

From the above results, two are concluded. First, the overall reaction is

reversible, while the discharged product is Li_2S and charged product is sulfur. Second, discharged/charged phases are influenced by the type of sulfur-carbon composite and electrolyte, since dissolved intermediates are sensitive to their environment. So, it is important to specify dissolved intermediates. To do this other than structural analysis is needed.

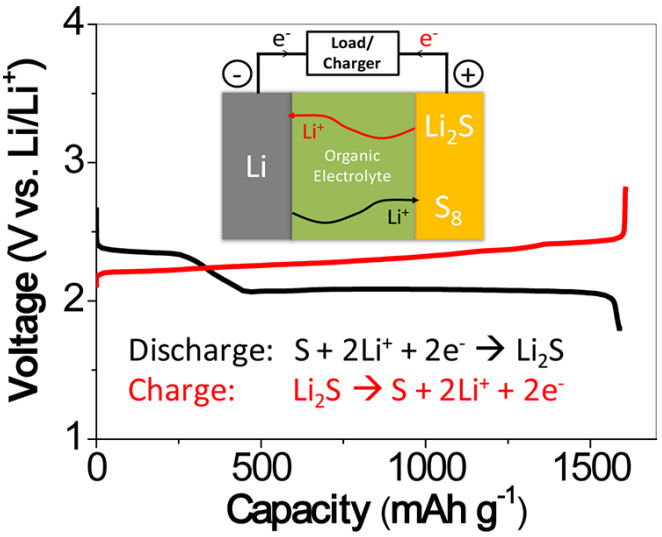

Fig. 2.1. Discharge/charge profile of liquid state Li-sulfur battery [8]

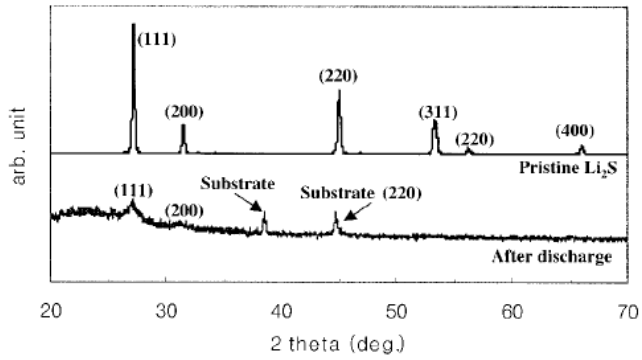

Fig. 2.2 Ex-situ XRD profile of discharged cathode (at 1.5 V) [10]

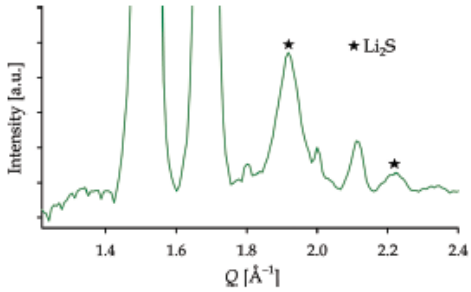

Fig. 2.3 Ex-situ XRD profile of discharged cathode (to 1043 mAh g^{-1}) [13]

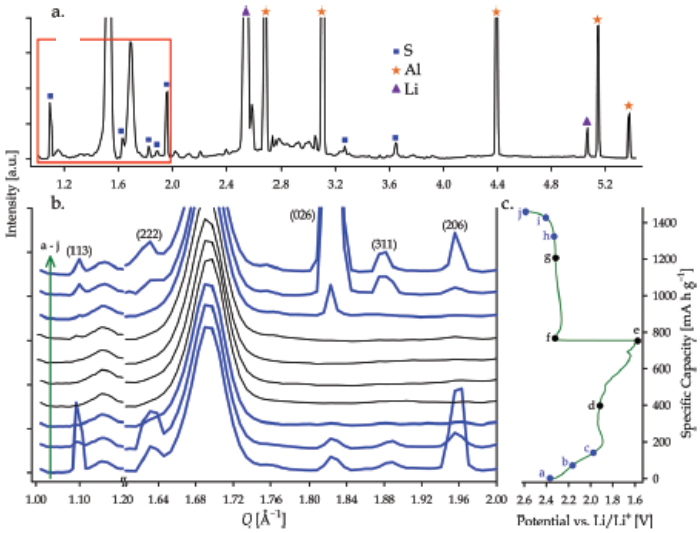

Fig. 2.4 In-situ XRD profile of cathode [13]

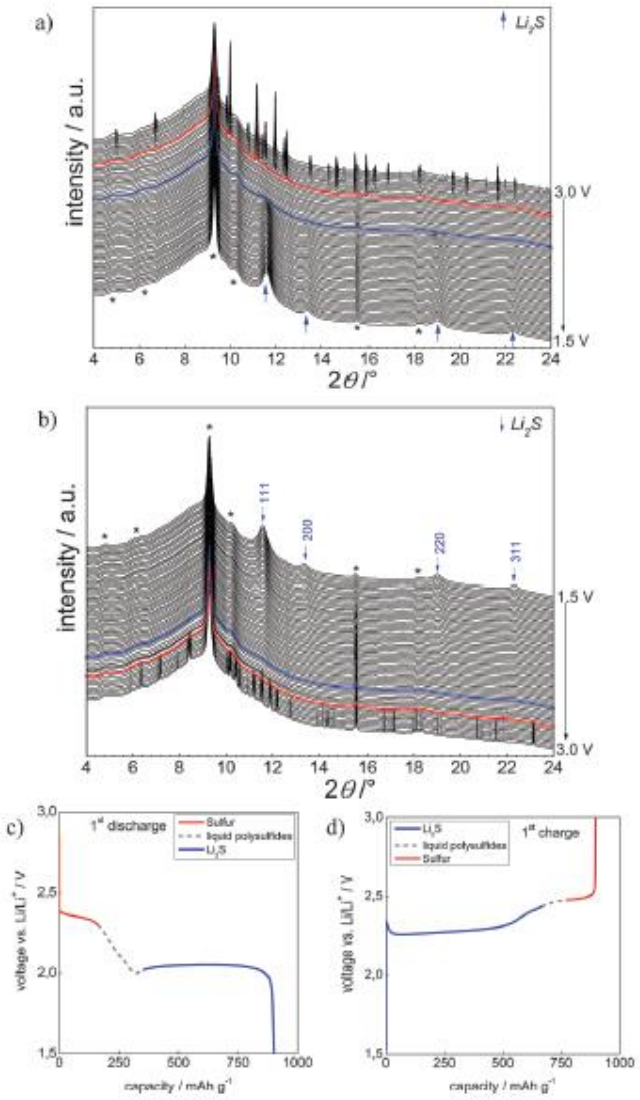

Fig. 2.5 In-situ XRD profile of cathode [14]

In 2003, S.-E. Cheon et al. [10] showed there is no sulfur atom containing intermediates of the discharge/charge process. Since lithium polysulfides are soluble [15], intermediates can be suspected as soluble lithium polysulfides.

In 2008, K. Kumareasan et al. suggested several polysulfides' reactions and solved differential equations [16]. The discharge profile produced by the calculation was same with the experimental results. This result also expects that the intermediates are lithium polysulfides in a roundabout way.

In 2012, C. Barchasz et al. used UV-vis absorption spectroscopy, high-performance liquid chromatography (HPLC), and electron spin resonance (ESR) spectroscopy to detect soluble intermediate species [17]. Li_2S_8 was synthesized by dissolving sulfur and Li metal (8:2 by weight ratio) in TEGDME which works as an active material for a cathode. LiTFSI was added to the solution until the salt concentration reached 1 mol L^{-1}. A Pt foil works as a working electrode, while a Li metal as both a counter and a reference electrode. Constant voltage was applied until the current decreases below 10 μA and ex-situ measurements were applied. Fig. 2.6 shows UV-vis absorption spectra and Fig. 2.7 shows HPLC spectra. From Fig. 2.6 A, B, C, S_6^{2-} and S_5^{2-} peaks were found and grew during 1st discharge plateau. We can speculate S_8^{2-} was generated from S_8 during 1st plateau and was chemically reacted to S_6^{2-} and S_5^{2-}. From Fig. 2.6 E, S_6^{2-} and S_5^{2-} peaks were declined and S_3^{2-} and S_4^{2-} peaks were rising. It means that S_6^{2-} and S_5^{2-} were consumed and S_3^{2-} and S_4^{2-} were produced during sloppy region. From Fig. 2.7 peaks attributed by S_5^{2-}, S_4^{2-}, S_3^{2-}, and S_2^{2-} disappeared during 2nd discharge plateau. Since those

polysulfides reacted to form partially soluble or insoluble S_3^{2-}, S_2^{2-}, and S^{2-}.

In the same year, J.-T. Yeon et al. identified soluble intermediate species by ex-situ Raman spectroscopy [18]. The cathode was composed by sulfur, super P, PVdF (7:2:1 by weight ratio). The electrolyte was 1 M LiTFSI in TEGDME:DOL (40:60 by volume) and the anode was Li metal. Fig. 2.8 (b) shows Raman spectra at the points in Fig. 2.8 (a). Sulfur disappeared during discharge and reappeared during charge. Polysulfides was generated during discharge and charge. Though Li_2S was not detected by Raman spectroscopy, it was identified by ex-situ XRD as previous reports. Remaining polysulfides at the end of charge were related to the capacity decaying.

By these efforts, first, lithium polysulfides (Li_2S_n, $2 \leq n \leq 8$) are intermediate species. They exists as liquid phase due to high solubility in electrolyte [15]. Second, their reaction occurs almost simultaneously. It is consistent with that the equilibrium potentials of these lithium polysulfides are similar [19]. Third, reaction of soluble lithium polysulfides is easily affected by the environment and sometimes several plateaus appear [20, 21].

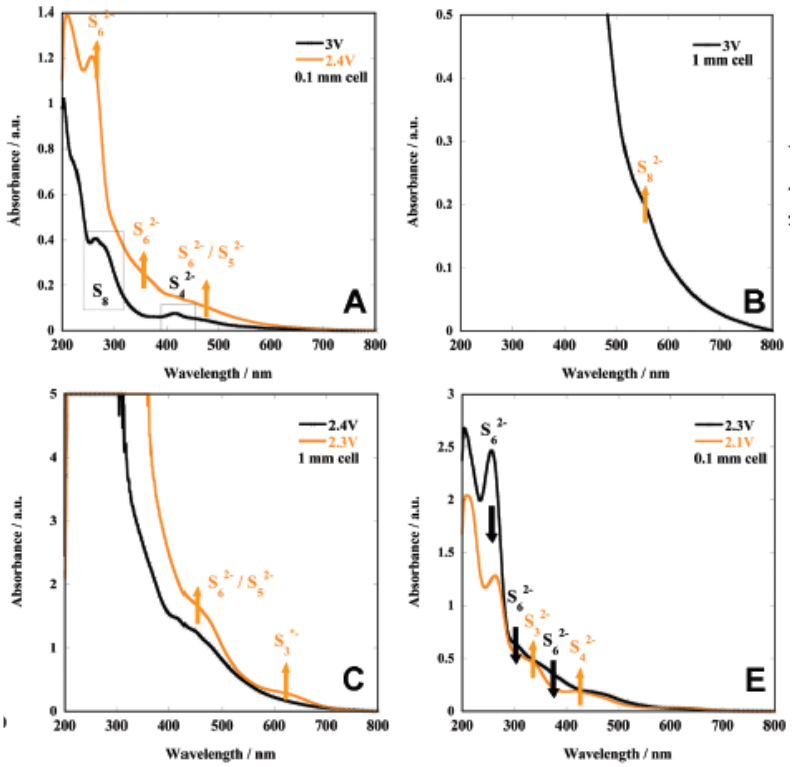

Fig. 2.6 UV-vis absorption spectra [17]

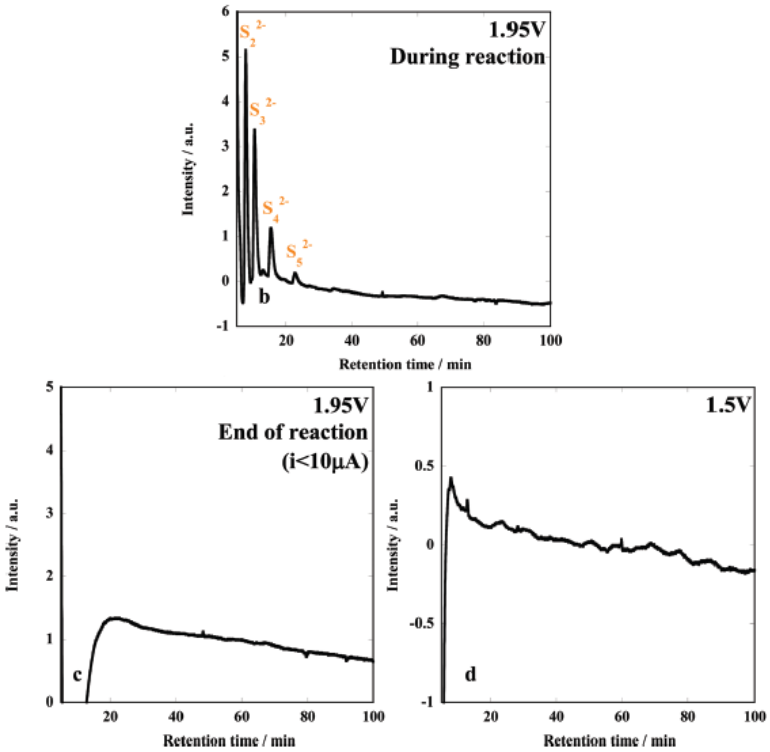

Fig. 2.7 HPLC spectra [17]

(a)

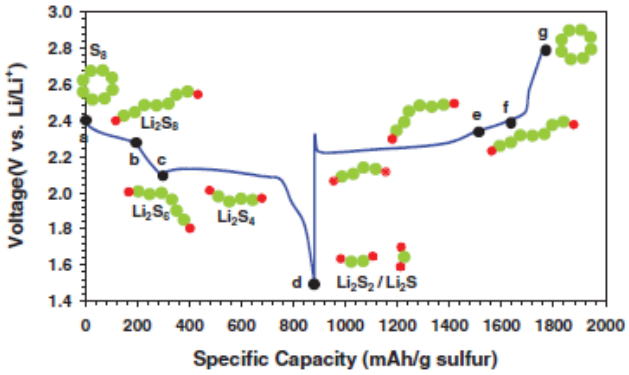

(b)

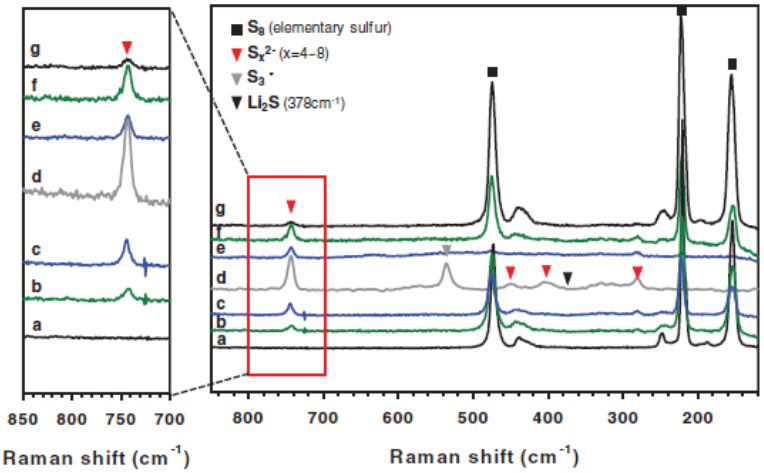

Fig. 2.8 (a) First discharge and charge profiles (cut off: 1.5 V-2.8 V, C-rate: C/20) with ex-situ measurement points. (b) Ex-situ Raman spectra. (a- pristine cathode. b- at 2.28 V. c- at 2.1 V. d- full discharge. e- at 2.34 V. f- at 2.4 V. g- full charge.) [18]

2.1.2 Researches in Li-sulfur battery

Li-sulfur battery has promising conditions such as high energy density, low cost, and environmentally friendliness. Fig. 2.8 is a conventional discharge/charge profile of Li-sulfur battery. However, several disadvantages obstruct commercialization of Li-sulfur battery. First, sulfur and its discharged products have low electronic conductivity. The electronic conductivity of sulfur is $5x10^{-30}$ S cm^{-1} and Li_2S is $3.6x10^{-7}$ S cm^{-1} at 25 ℃ [18]. Because of the low electronic conductivity, sulfur cathode contains about 40 wt% of carbon which is higher than conventional cathode. Also, it is usual that cathode of Li-sulfur battery uses sulfur-carbon composite. Second, electrochemical reaction of sulfur (2.07 g cm^{-3}) to Li_2S (1.66 g cm^{-3}) accompanied 80 % volume expansion. Due to the volume expansion, reorganization of the cathode and degradation of the cell performance exist. Third, intermediate lithium polysulfides (Li_2S_n, $2 \leq n \leq 8$) dissolve in the liquid electrolyte. With the first problem, as the cycle passes, the separation of carbon and sulfur increases as shown in Fig. 2.9 which causes cyclability and capacity degrade [22]. Side reaction, called shuttle mechanism is caused by soluble lithium polysulfides. Shuttle mechanism is the circuit of the reaction as shown in Fig. 2.1. Diffused soluble long-chain lithium polysulfides reduced at the anode and forms short-chain polysulfides which will be diffuse back to the cathode to be oxidized to long-chain polysulfides. C. Barchasz et al. confirmed S_8^{2-} after 100 hrs of the cell at 3 V vs. Li/Li^+ which is even higher than the equilibrium oxidation potential (2.4 V) [17] . Also, the current did not

fall down to zero due to the shuttle mechanism.

Dissolution of the polysulfides is the main reason for poor cyclability. First, some scientists focus on cathodes which is the most popular research area. Some researchers make containers to prevent diffusion of the polysulfides and to minimize volume expansion as shown in Fig. 2.11. Since sulfur melt at relatively low temperature (120 ℃), sulfur-container composite is easily synthesized by entering melted sulfur into pores of the containers by the capillary effect. Most usual container is carbon that can also improve electronic conductivity [23, 24, 25]. Also, polymer shell such as poly-acrylonitrile (PAN) [26, 27], polyvinyl-pyrrolidone (PVP) [28] and ceramic shell such as TiO_2 [29, 30], $FePO_4$ [31] were used. Other scientists use cross-linking binders [32] or viscous catholyte [33, 34, 35] to hinder polysulfdies' diffusion.

Second, other researchers concentrate on anodes prevention. $LiNO_3$ [36] and phosphorous pentasulfide [37] were studied as additives which passivate Li anode. Y.-S. Su et al., inserted carbon paper to prevent diffusion of polysulfides [38]. However, consumption of the additives and contamination of the inserted carbon paper during cycling need improvements.

Third, some scientists consider the electrolytes which are the root for solubility of the lithium polysulfides. Various combinations of solvents and salts for liquid electrolytes were explored for better electrochemical performance [39, 40]. Today, other than carbonate liquid electrolytes [41] are mixed and used with additives in liquid state Li-sulfur battery system. Either of the combination could not completely prevent the solvation of polysulfdies

and some researchers try to adapt solid electrolytes. Considering proper Li ionic conductivity and electrochemical stability thio-LiSICON type solid electrolyte was popularly used in Li-sulfur battery such as Li_2S-P_2S_5 [42, 43, 44] and β-Li_3PS_4 [45].

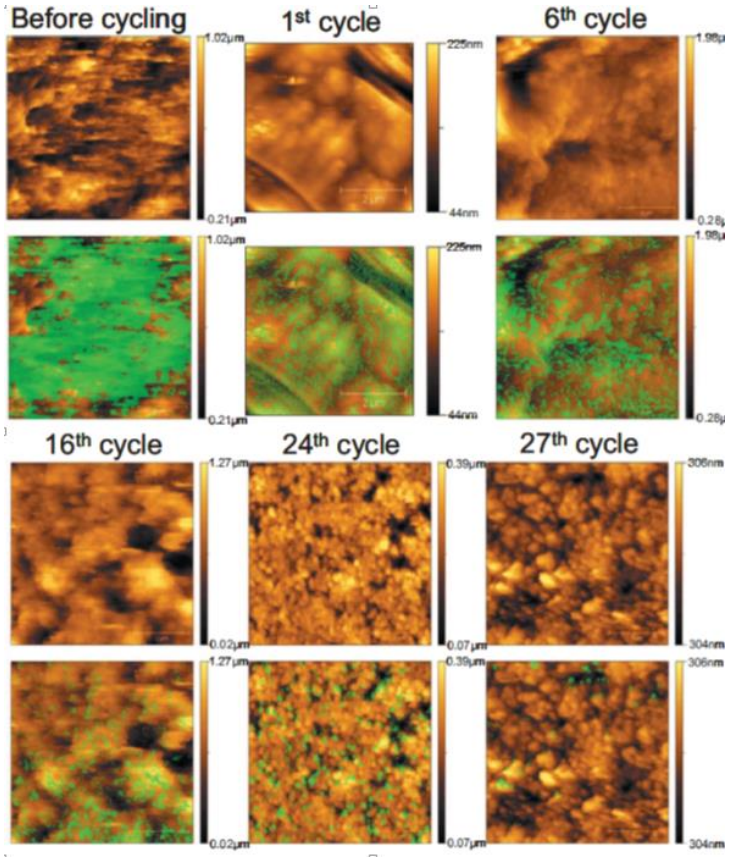

Fig. 2.9 AMF topography (top) and conductivity (bottom) images of sulfur cathodes (different numbers of cycles is indicated) [22]

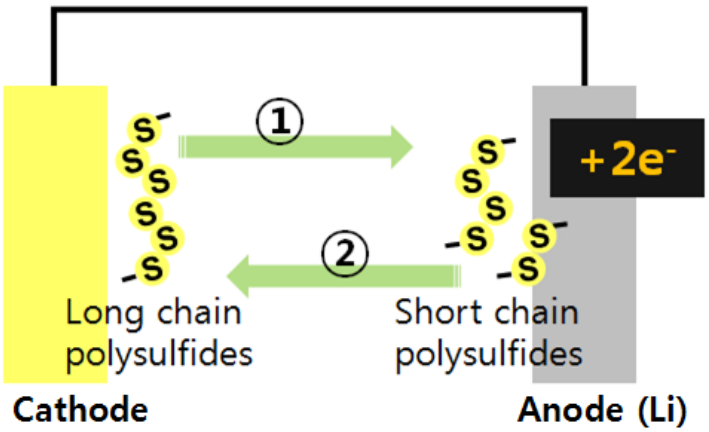

Fig. 2.10 Schematic of shuttle mechanism

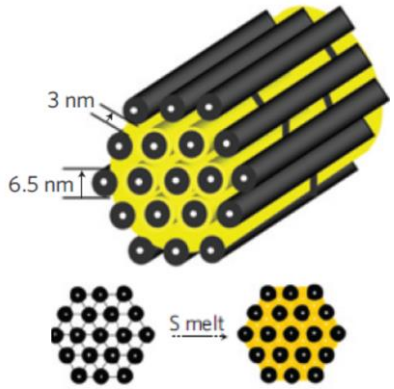

Fig. 2.11 Schematic of infiltrated sulfur into CMK-3 container [23]

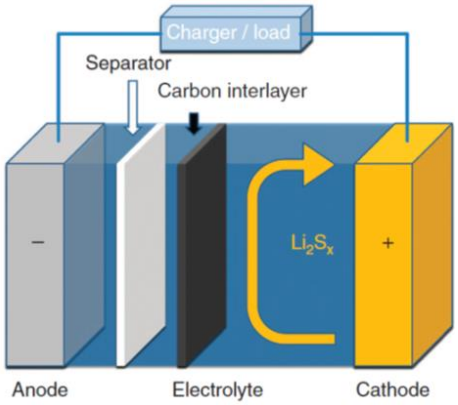

Fig. 2.12 New system of Li-sulfur battery with (a) inserted carbon paper. (b) catholyte. (c) cross-linking binder [38]

2.2 Thio-LiSICON analogue solid electrolyte

Thio-LiSICON family is expressed by a general formula, $Li_{4-x}M_{1-y}M'_yS_4$ with M(IV)= Si, Ge, M'(V or III)= P, Al, Zn, Ga [46]. Thio-LiSICON is named from the structural similarity to LiSICON ($Li_{14}Zn(GeO_4)_4$) [46]. Ionic conductivity is affected by the size and polarizability of the constituent ions, or interstitial-vacancy ordering caused by the substitutions [46]. So, Thio-LiSICON which consists of polarizable sulfur atoms usually has higher ionic conductivity than LiSICON which consists of smaller oxygen atoms.

Fig. 2.13 shows the structure of Li_4GeS_4. This structure is the base of thio-LiSICON structure. The structure is composed of hexagonal close-packed sulfide ion arrays, and the lithium and M/M' ions are distributed over the tetrahedral and octahedral sites [47]. The Li^3S_6 octahedra are connected with each other by sharing edges and forming chain along the b-axis [47]. Li^1S_4 tetrahedra are connected with the Li^3S_6 octahedra by sharing edges, while the Li_2S^4 tetrahedra are linked to the Li^3S_6 octahedra by sharing faces [47]. The $Li^{1*}S_4$ tetrahedra are interstitial sites between Li^3S_6 chains and Li^1S_4 tetrahedra [47].

Fig. 2.14 shows the Li ion conduction path of thio-LiSICON structure and Table 2 shows Li ion occupation parameters [47]. For Li_4GeS_4, the occupation parameters of Li^1, Li^2, and Li^3 sites are almost 1, while that of Li^{1*} sites are 0 [47]. For Li_3PS_4, the occupation parameters of Li^{1*}, Li^2, and Li^3 sites are 0.28, 1, and 0.68, while that of Li^1 sites are 0. Li ionic conductivity is affected by the Li ion distribution. (Li_4GeS_4~$2.0x10^{-7}$ S cm^{-1} *vs.*

Li_3PS_4~$3.0x10^{-7}$ S cm^{-1}) [47]. The highest ionic conductivity was observed at x= 0.75 in the solid solution $Li_{4-x}Ge_{1-x}P_xS_4$ [47], due to the cation ordering at the tetrahedral sites as for Li_4GeS_4 and Li_3PS_4.

The solid solution phase thio-LiSICON can be modified by Li_2S-P_2S_5 simple binary system, called thio-LiSICON analogue. For example, α-Li_2S(80 mol%)-P_2S_5(20 mol %) crystallizes to $Li_{3.25}P_{0.95}S_4$ which is similar to thio-LiSICON II ($Li_{3.25}Ge_{0.25}P_{0.75}S_4$) after a heat treatment [48].

This thio-LiSICON analogue has several advantages. First, it has a high Li ionic conductivity (thio-LiSICON II analogue Li_2S(80 mol%)-P_2S_5(20 mol%)~$7.2x10^{-4}$ S cm^{-1}) [48]. Second, since there is no metal component, contact with Li metal is stable. Third, it has wide voltage window as shown in Fig. 2.15 [46].

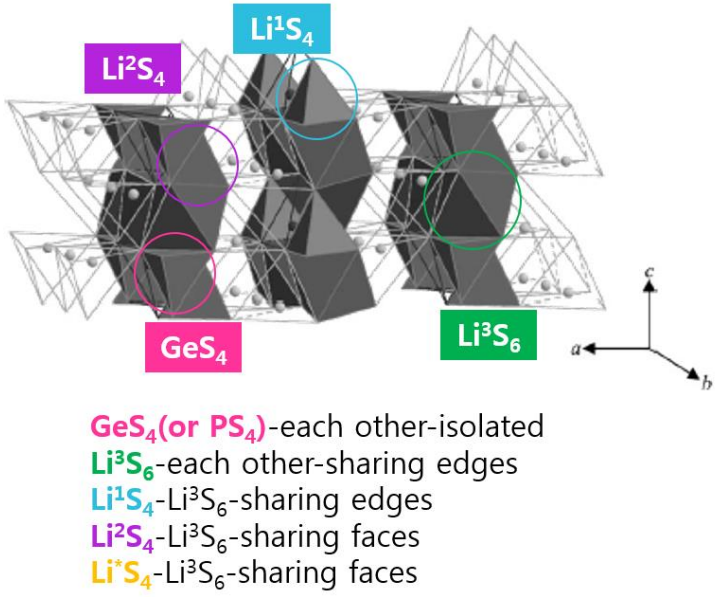

Fig. 2.13 Structure of Li_4GeS_4 which is the base structure of thio-LiSICON [47]

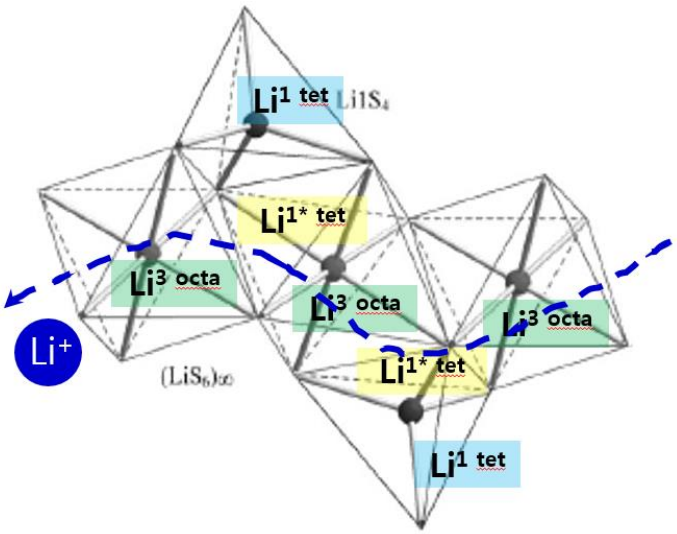

Fig. 2.14 Li ion conduction path of thio-LiSICON structure [47]

	Li^{1} tet	Li^{1*} tet	Li^{2} tet	Li^{3} octa
Li_4GeS_4	1.002	0	0.995	1.013
Li_3PS_4	0	0.28	1	0.68

Table 2 Li ion occupation parameters of Li_4GeS_4 and Li_3PS_4

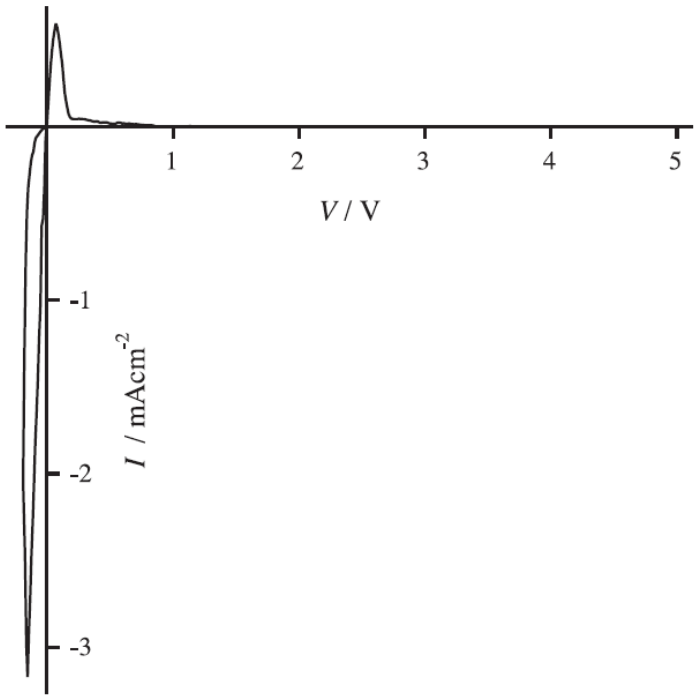

Fig. 2.15 Cyclic voltammogram of the cell, Li/$Li_{3+5x}P_{1-x}S_4$/SUS, using reference Li electrode [46]

2.3 Research background

The most important problem for Li-sulfur battery is poor cycle life caused by dissolution of intermediates. Polar intermediates are soluble in liquid electrolyte, due to the polar component which keeps Li ionic conductivity. In order to overcome this problem of liquid electrolyte, solid electrolyte is suggested as a solution. Since the study on all-solid-state Li-sulfur battery is in its infant stage, more efforts should be concentrated on the analysis of mechanism on all-solid-state Li-sulfur battery.

In 2010, T. Takeuchi et al. reported all-solid-state Li-sulfur battery mechanism [49]. Li_2S and Acetylene black (1:1 by weight ratio) were treated by the spark-plasma-sintering (SPS) process to obtain composite. The cathode was composed of Li_2S-C composite and solid electrolyte (0.01 Li_3PO_4-0.63Li_2S-0.36SiS_2) (3:7 by weight ratio), while the anode with indium (In) metal. The C-rate was 0.01 C (1 C= 1163 mAh g^{-1}).

Fig. 2.16 shows charge/discharge profile for the Li_2S/In cell which has only one plateau at 2.1 V vs. Li. This result suggests that the electrochemical reaction of all-solid-state Li-sulfur battery is different from that of liquid state Li-sulfur battery.

Fig. 2.17 shows ex-situ XRD profiles. In this figure, Li_2S peaks were drastically reduced, where sulfur peaks were not detected after 1st charge. This might be due to the low crystallinity of the formed elemental sulfur. Li_2S peaks were raised after 1st discharge. The intensity of Li_2S main-peak was significantly decreased compared with that of as-prepared sample. It might be

due to the low crystallinity of the Li_2S resulted after 1st charge. The same tendency of 2nd charge/discharge XRD profile implies that the electrochemical reaction is reversible ($2Li + S \leftrightarrow Li_2S$).

Fig. 2.18(a) shows S-K edge X-ray absorption fine structure (XAFS) spectra. Absorption peak at 2470~2747 eV is originated from the 1s →3p electronic transition in sulfur atoms. Since the 1s →3p electronic transition in S^0 occurs more frequently than that in S^{2-}, absorption peak height has correlation with the oxidation state of sulfur atoms. It can be concluded that reversible S^0/S^{2-} reaction occurred in all-solid-state Li-sulfur battery. The difference in radial structure function (RSF) was obtained by transforming XAFS results as shown in Fig. 2.18(b). The result shows that sulfur was formed after 1st charge, while Li_2S after 1st discharge. From 2nd charge spectrum, lithium deficient Li_2S might be formed and the reaction is incomplete reversible.

XRD measurement is beneficial to identify crystal structure but, not appropriate to analyze non-crystalline polysulfides. XAFS is suitable for examining change in oxidation state but, not in measuring quantity of the shift.

In this thesis, Raman spectroscopy and X-ray photoelectron spectroscopy (XPS) was used, which can detect polysulfides as well as sulfur and Li_2S. Especially, from deconvolution of XPS spectra predicts various intermediates.

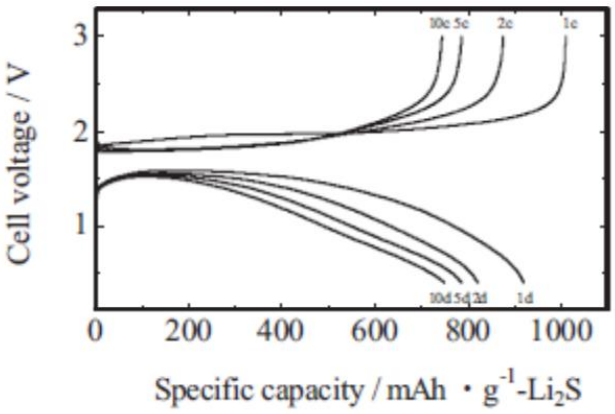

Fig. 2.16 Charge/discharge profile of all-solid-state Li-sulfur battery [49]

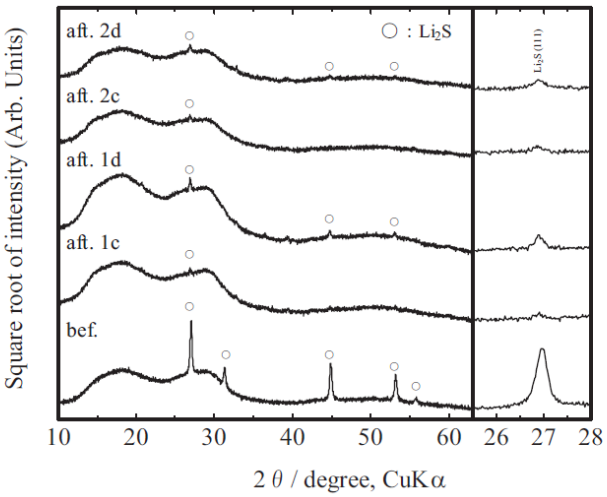

Fig. 2.17 Ex-situ XRD profile of all-solid-state Li-sulfur battery [49]

(a)

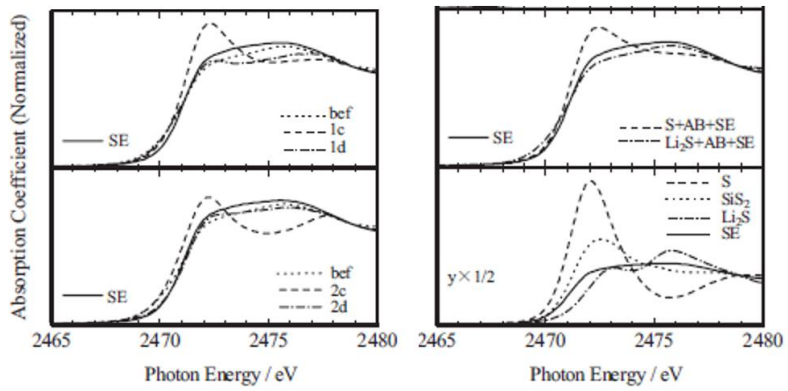

(b)

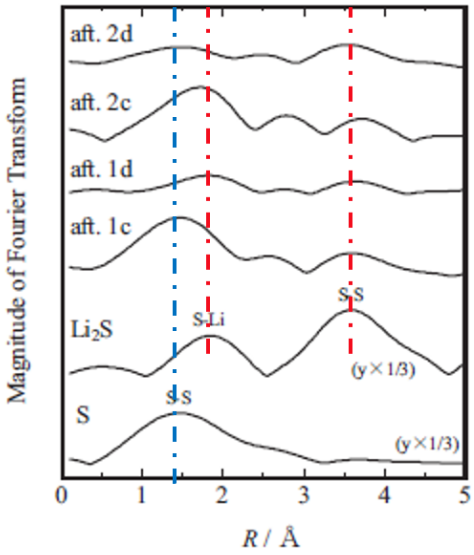

Fig. 2.18 (a) S-K edge XAFS spectra. (b) RSF graph [49]

Chapter 3. Experimental section

3.1 Synthesis and characterization of thio-LiSICON II analogue phase solid electrolyte

Li_2S(Aldrich) and P_2S_5 (Aldrich) grinded with 80 mol%:20 mol% ratio. The grinded precursor was mechanically milled at 370 rpm for 20 hrs to synthesize amorphous Li_2S-P_2S_5. The synthesized amorphous Li_2S-P_2S_5 was heat treated at 210 ℃ for 1 hr in Ar atmosphere to synthesize Thio-LiSICON II analogue phase Li_2S-P_2S_5.

Structure of the synthesized phase is confirmed by XRD measurement. Li ionic conductivity was measured by electrochemical impedance spectroscopy (EIS) and cell construction was as shown in Fig. 3.1.

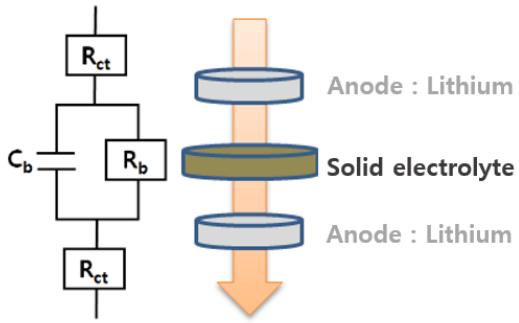

R_b: Li conduction in a solid electrolyte
C_b: Li storage in grain boundary inside a solid electrolyte
R_{ct}: Li ⇄ $Li^+ + e^-$ reaction at the interface

Fig. 3.1 Cell construction for EIS measurement

3.2 Cell fabrication and characterization of thio-LiSICON II analogue phase for Li-sulfur batteries

Since all-solid-state Li ion battery do not have regularized cell construction as in liquid state Li ion battery (coin cell), we have to find suitable cell construction by trial and error.

Fig. 3.2 is schematic of Swagelok (Type III) cell construction. Solid electrolyte (0.078 g) was pressed by 10 MPa in a Swagelok mold. Ball-milled sulfur: super P: solid electrolyte (1:1:2 by weight ratio) (0.015 g) was pressed by 20 MPa to make cathode-solid electrolyte bi-layer. Al mesh current collector was pressed by 30 MPa on the cathode side to improve electrical contact between SUS electrode and cathode layer. Li metal was attached on the solid electrolyte side.

Fig. 3.3 is a schematic of 2032 (Type II) cell construction. Al mesh current collector-cathode-solid electrolyte layered structure which was produced as above was detached from a Swagelok mold. Cell was constructed by 2032 coin cell assembler with 0.8 t spacer and Li metal as an anode.

Fig. 3.4 is a schematic of 2032 (Type IV) cell construction. Ball-milled Li_2S: super P: solid electrolyte (1:1:2 by weight ratio) was used as a cathode. Al mesh current collector-cathode-solid electrolyte layered structure which was produced as above was detached from a Swagelok mold. Cell was constructed by 2032 coin cell assembler with 0.8 t spacer and In metal (0.1 mm thick) as an anode.

Raman spectroscopy measurement and XPS measurement was conducted to 2032 (Type IV) cell to confirm the mechanism of thio-LiSICON II

analogue phase for Li-sulfur battery.

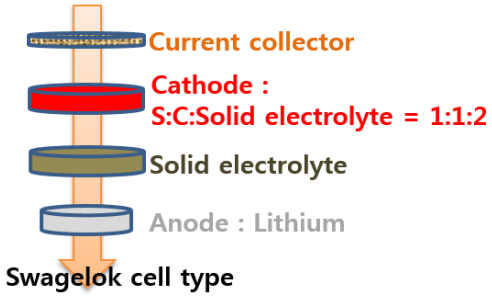

Fig. 3.2 Schematic of Swagelok (Type III) cell construction

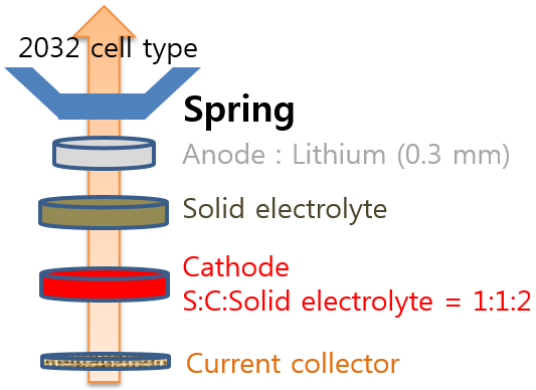

Fig. 3.3 Schematic of 2032 (Type II) cell construction

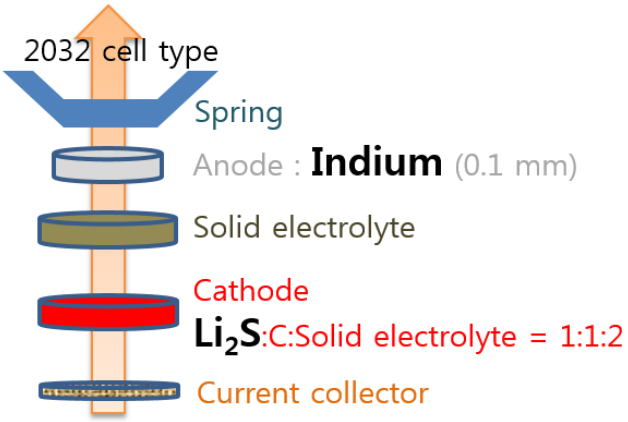

Fig. 3.4 Schematic of 2032 (Type IV) cell construction

Chapter 4. Results and Discussion

4.1 Characterization of thio-LiSICON II analogue phase solid electrolyte

4.1.1 Structure of the synthesized solid electrolyte

Fig. 4.1 (a) shows XRD profile of grinded precursors, Li_2S (Aldrich) and P_2S_5 (Aldrich). Precursor Li_2S (Aldrich) shows high crystallinity. Though P_2S_5 is known to be crystalline, precursor P_2S_5 (Aldrich) did not show significant peaks. Fig. 4.1 (b) shows XRD profile of mechanically milled Li_2S(80 mol%)-P_2S_5(20 mol%) at 370 rpm for 20 hrs. Li_2S and P_2S_5 powder were pulverized and the atoms diffused at the interface to make amorphous phase. Li_2S peaks' intensity are significantly decreased. However, reaming Li_2S peaks are in coincident with previous literature [45]. Fig. 4.1 (c) shows heat treated amorphous Li_2S(80 mol%)-P_2S_5(20 mol%) at 210 ℃ for 1hr to transform into thio-LiSICON analogue. The peak profile of the composite is consistent with previous result [46].

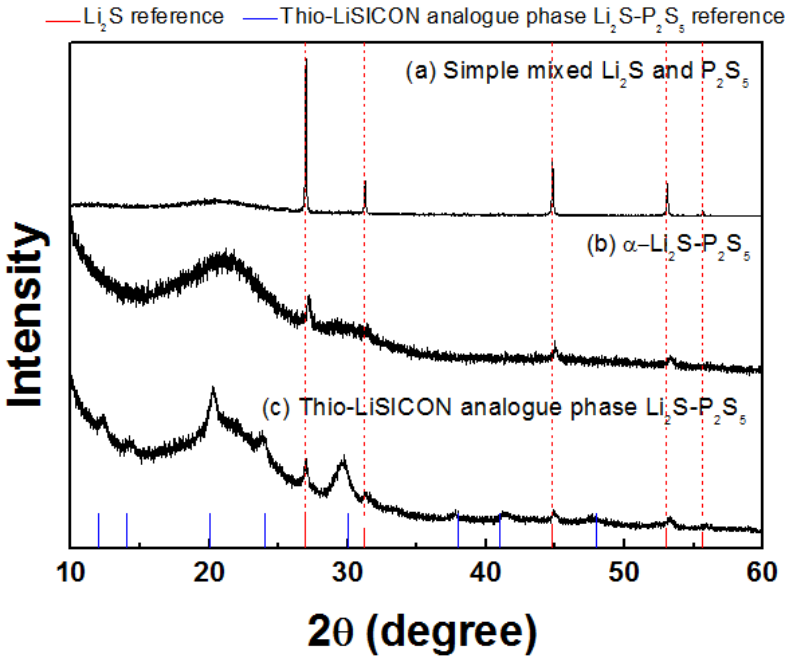

Fig. 4.1 XRD profile of **(a)** grinded precursors, Li_2S (Aldrich) and P_2S_5 (Aldrich). (b) mechanically milled Li_2S(80 mol%)-P_2S_5(20 mol%). (c) heat treated amorphous Li_2S(80 mol%)-P_2S_5(20 mol%)

4.1.2 Li ionic conductivity of the synthesized solid electrolyte

Fig. 4.2 shows EIS measurement result. Start point of the semicircle represents R_{ct} (resistance of the charge transfer reaction: $Li \leftrightarrow Li^+ + e^-$). Diameter of the semicircle represents R_b (resistance of the bulk solid electrolyte). So, R_{ct} is 200 Ω and R_b is 850 Ω. Since $R=\rho L/A$, $\sigma=1/\rho$ (R=resistance, ρ=resistivity, σ= conductivity, A= area of the resistive material, L=thickness of the resistive material), Li ionic conductivity of the synthesized bulk solid electrolyte is 4.3×10^{-5} S cm^{-1}. Though reported Li ionic conductivity of the thio-LiSICON II analogue Li_2S(80 mol%)-P_2S_5(20 mol%) was 7.2×10^{-4} S cm^{-1} [48], that of the synthesized solid electrolyte is still proper to be used as an electrolyte. The difference may be due to the interface resistance which is caused by insufficient pressure applied to solid electrolyte pellet [50].

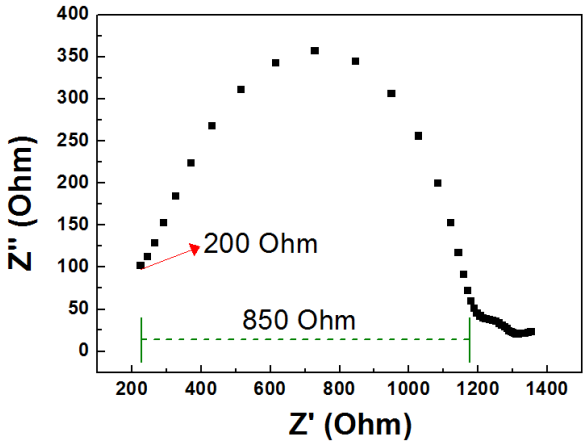

Fig. 4.2 EIS measurement result

4.2 Characterization of thio-LiSICON II analogue phase for Li-sulfur batteries

4.2.1 Electrochemical properties of Swagelok (Type III) cell

Fig. 4.3 shows discharge/charge profile of Swagelok (Type III) cell (Cut off: 1.0 V- 3.0V vs. Li, C-rate: 0.01 C where 1 C =1673 mA g^{-1}, at 25 ℃). The 1st discharge capacity (40 mAh g^{-1}) was very small compared to the theoretical capacity (1673 mAh g^{-1}). Charge did not work correctly. It discharged below 1.5 V and charged above 2.5 V (high polarization). It is expected that the results are caused by poor contact between electrolyte and electrode due to volume change of active material. For improvement of the electrochemical properties the variation in volume should be simultaneously adjusted.

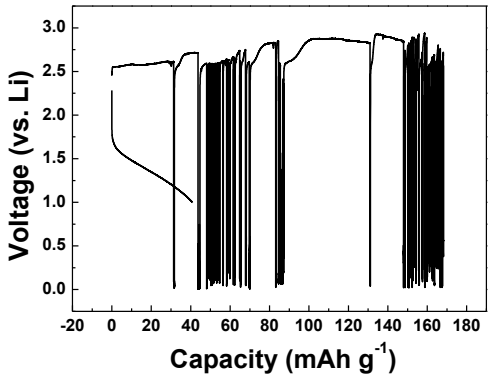

Fig. 4.3 discharge/charge profile of Swagelok (Type III) cell (Cut off: 1.0 V-3.0V vs. Li, C-rate: 0.01 C where 1 C =1673 mA g^{-1}, at 25 ℃)

4.2.2 Electrochemical properties of 2032 (Type II) cell

Fig. 4.4 shows discharge/charge profile of 2032 (Type II) cell (Cut off: 1.0 V- 3.0 V vs. Li, C-rate: 0.01 C where 1 C =1673 mA g^{-1}, at 60 ℃). Spring in 2032 coin cell was applied to mitigate the volume variation problem of the Swagelok (Type III). The 1st discharge capacity increased to 400 mAh g^{-1}. The 1st charge capacity also increased to 600 mAh g^{-1} but, instability in profile was not remarkably removed. Referring to the literature written by M. Hiratani et al. [51] we can assumed that the remaining instability is due to the Li charge transfer resistance at solid electrolyte-Li metal interface.

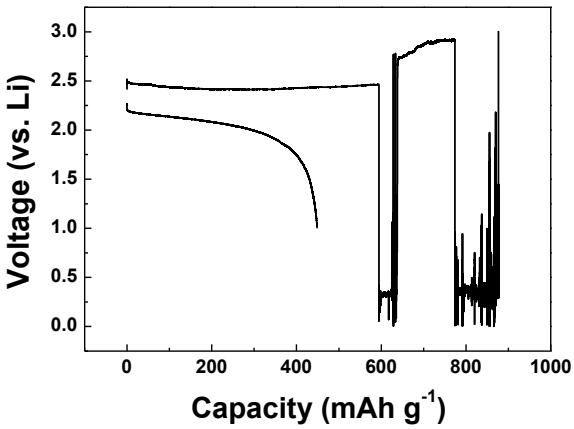

Fig. 4.4 discharge/charge profile of 2032 (Type II) cell (Cut off: 1.0 V- 3.0V vs. Li, C-rate: 0.01 C where 1 C =1673 mA g^{-1}, at 60 ℃)

4.2.3 Electrochemical properties of 2032 (Type IV) cell

Fig. 4.5 shows charge/discharge profile of 2032 (Type IV) cell (Cut off: 0.5 V- 2.5 V (1.0 V-3.0 V vs. Li), C-rate: C/70 (0.014 C) where 1 C =1163 mA g^{-1}, at 60 ℃). Li_2S is used as a cathode active material and In as an anode material. Li-solid electrolyte interface was improved by electrically formed InLi alloy to eliminate remaining instability in Fig. 4.4. As expected, instability during electrochemical reaction was disappeared. The 1st charge capacity is 900 mAh g^{-1} which is close to the theoretical capacity. The 1st discharge capacity is 447 mAh g^{-1}. The unbalance between charge and discharge capacity might be due to the reorganization of the cathode structure (interface between solid electrolyte-Li_2S-carbon). Large polarization during 1st charge is general property of Li_2S [52].

Fig. 4.6 (a) compares electrochemical profiles at different C-rate for 1st cycle. Fig. 4.6 (b) compares that for 2nd cycle. Fig. 4.6 (c) shows cyclability at different C-rates. Stable charge/discharge reaction was obtained in current density of C/20. Cyclability can be improved by solid electrolyte-Li_2S-carbon composite.

In Fig. 4.7, the ex-situ measurement points were added to the 1st cycle of Fig. 4.6 (a).

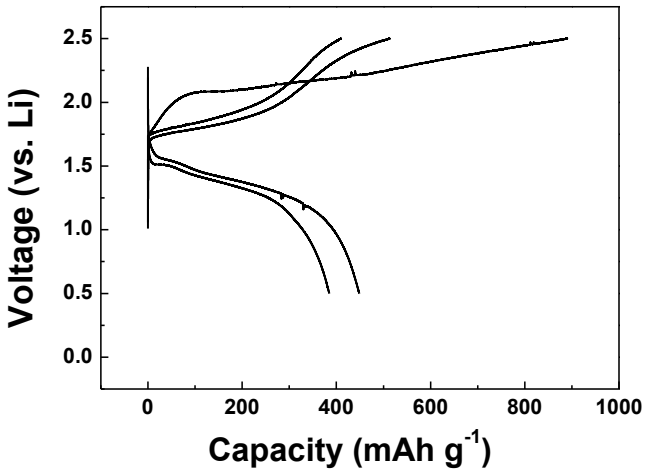

Fig. 4.5 charge/discharge profile of 2032 (Type IV) cell (Cut off: 0.5 V- 2.5V (1.0 V-3.0 V vs. Li), C-rate: C/70 (0.014 C) where 1 C =1163 mA g^{-1}, at 60 ℃)

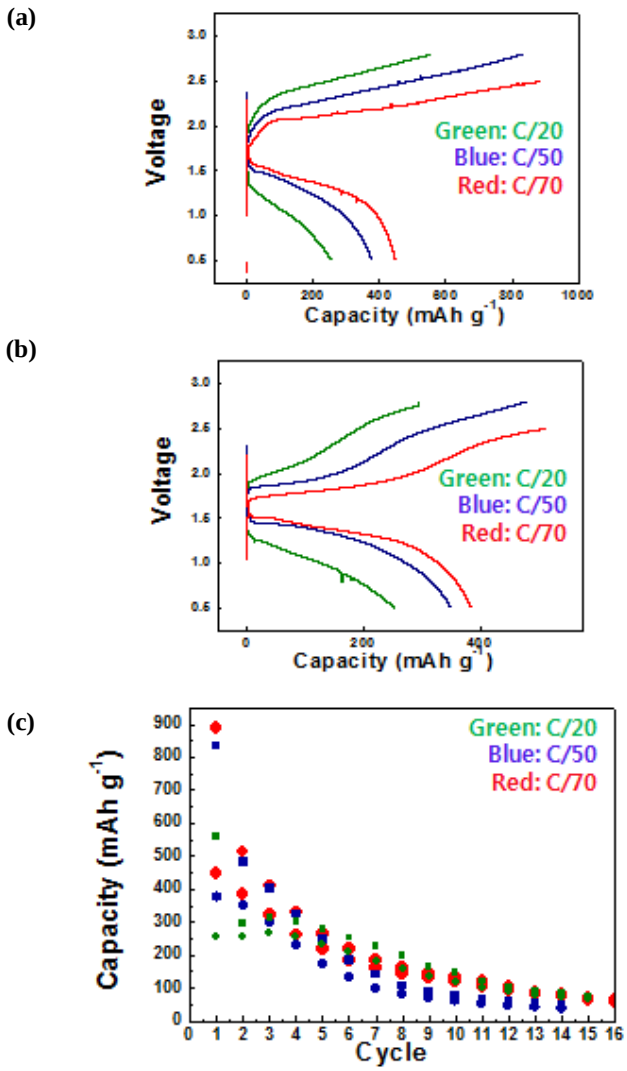

Fig. 4.6 Electrochemical profiles at different C-rate for (a) 1st cycle. (b) 2nd cycle. (c) cyclability at different C-rates.

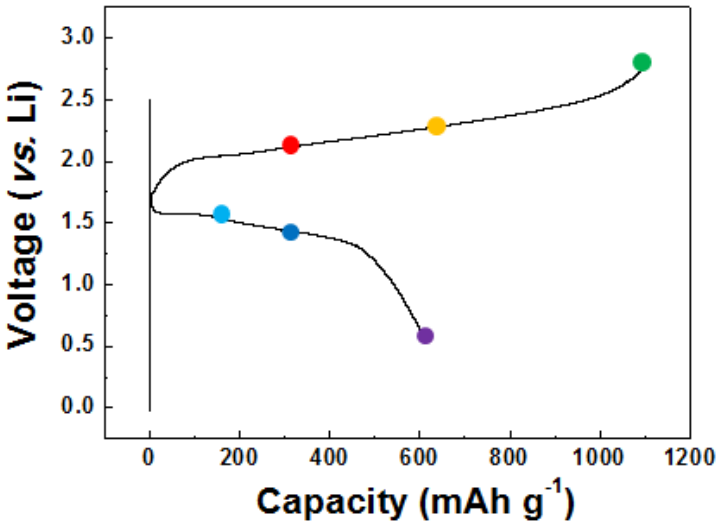

Fig. 4.7 Electrochemical profile of 1st cycle with ex-situ measurements points

4.2.4 Raman spectroscopy measurement

Table 3 shows the reference peak positions of sulfur [35], polysulfides [18], Li_2S [45] and PS_4^{3-} [45] of the solid electrolyte. Fig. 4.8 (b) is the ex-situ Raman spectra at the points in Fig. 4.7. Since as-prepared solid electrolyte has peaks at which polysulfides have peaks, it might be hard to figure out polysulfides unless the ratio of the active material in a cathode increases. After 1st charge, sulfur was observed, which was the charge product. All the sulfur was consumed during 1/3 depth of discharge.

	Peak position [cm^{-1}]
S-S bonding in S_8 [35]	155, 218/476, 248,437
S-S bonding in S_x^{2-}(x=4~8) [18]	280, 400, 450
Li-S bonding n Li_2S [45]	375
P-S bonding in PS_4^{3-} [45]	174, 295, 425

Table 3 Reference peak positions of sulfur, polysulfides, Li_2S and solid electrolyte

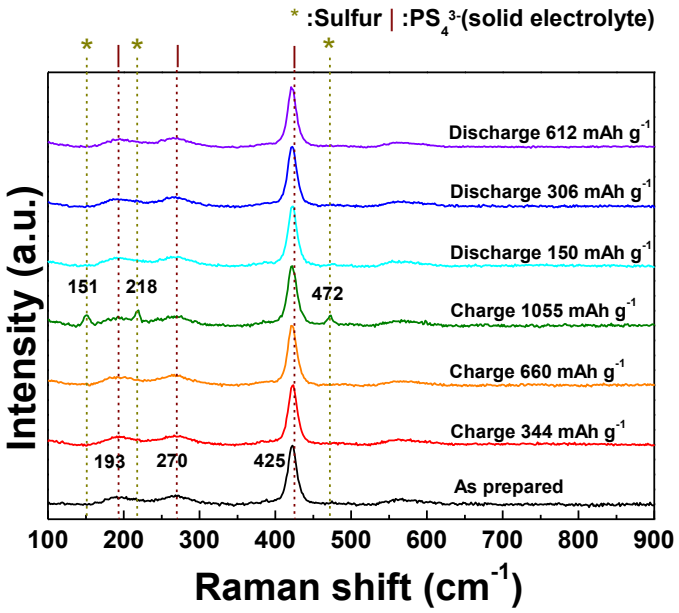

Fig. 4.8 Ex-situ Raman spectra at the points in Fig. 4.7

4.2.5 X-ray photoelectron spectroscopy measurement

Table 4 shows the reference peak positions of sulfur [35], lithium polysulfides [34, 53], and Li_2S [35]. Fig. 4.9 is the ex-situ XPS S 2p spectra at the marked points in Fig. 4.7. Peaks in Fig. 4.9 move to the left (oxidation) while charging and to the right (reduction) while discharge.

The result of the deconvolution of the peaks in Fig. 4.9 is shown in Fig. 4.10. Since XPS reference of the solid electrolyte was not reported, it was found by the deconvolution of the as-prepared sample. It is assumed 3-phases are in solid electrolyte (defective Li_2S, amorphous, crystalline).

First, lithium polysulfides' terminal peak (162.5 eV) appears during 1/3 depth of charge (at charge 333 mAh g^{-1}) in Fig. 4.10 (a) and sulfur in the middle of lithium polysulfides was not detected. From this result, lithium polysulfide does not exist in this stage. It is rather expected that defective Li_2S is formed at the initial state of charge, which has less Li in their environment as the sulfur in the end of lithium polysulfides.

Second, another lithium polysulfides' terminal peak (163.0 eV) with low intensity and lithium polysulfides' bridging peak (163.8 eV) with high intensity appear at the end of charge in Fig. 4.10 (a). It means that short-chain lithium polysulfides were formed [34].

Third, peak position shift in Fig. 4.10 (b) occurs in reverse order to that of Fig. 4. 10 (a). It means that the discharge is the reverse reaction of the charge.

Fourth, comparing as-prepared peaks in Fig. 4.10 (a) and peaks at last stage of the discharge (at discharge 612 mAh g^{-1}), there still remains lithium polysulfides' terminal peak at 162.5 eV. It means that the unbalance between charge and discharge capacity is from remaining defect in Li_2S.

By these results we suggest mechanism of the all-solid-state Li-sulfur battery as shown in Fig. 4.11. When charging, Li_2S oxidized to sulfur passing through defective Li_2S and later on to short-chain lithium polysulfides. Sulfur reduced to Li_2S in the reverse order while discharge. It is assumed that reorganization of the cathode during 1st charge causes defective Li_2S and poor electrochemical performance.

	Peak position [eV]
S_8 [35]	163.8, 165.1
$Li^+_2S_x^{2-}$(x=4~8) [34, 53]	162.4/162.9 (terminal) 163.7/164.0 (bridging)
Li_2S [35]	160.4, 161.9

Table 4 Reference peak positions of sulfur, polysulfides and Li_2S

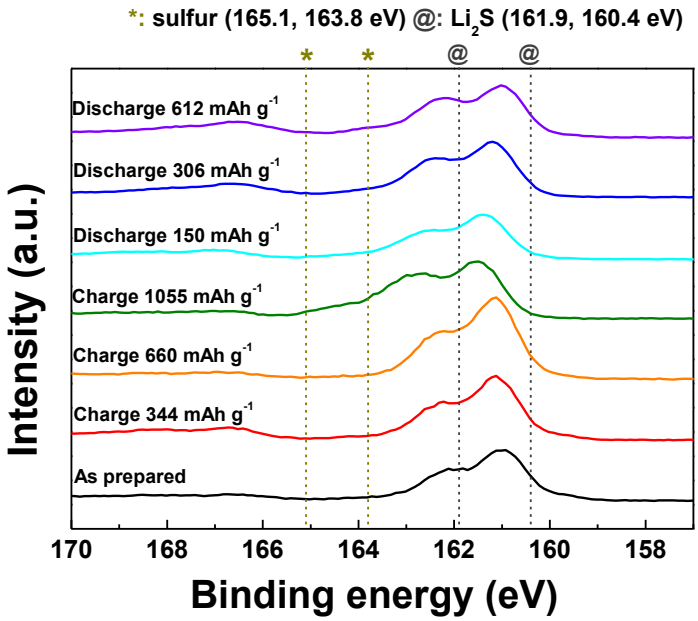

Fig. 4.9 Ex-situ XPS spectra at the points in Fig. 4.7

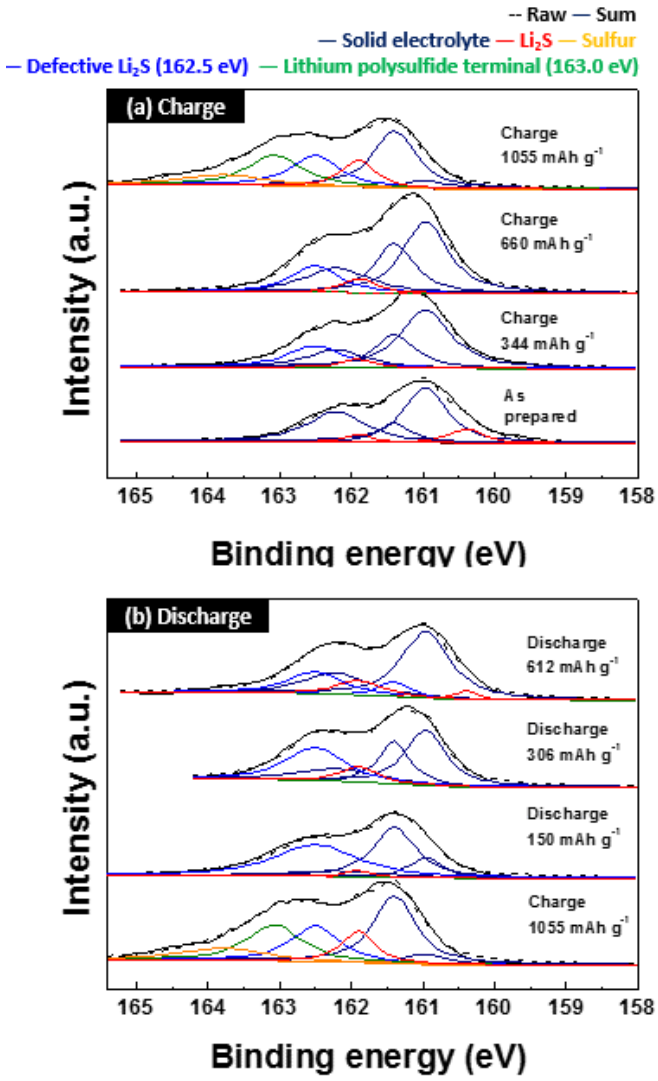

Fig. 4.10 Ex-situ XPS spectra after deconvolution during (a) charge. (b) discharge

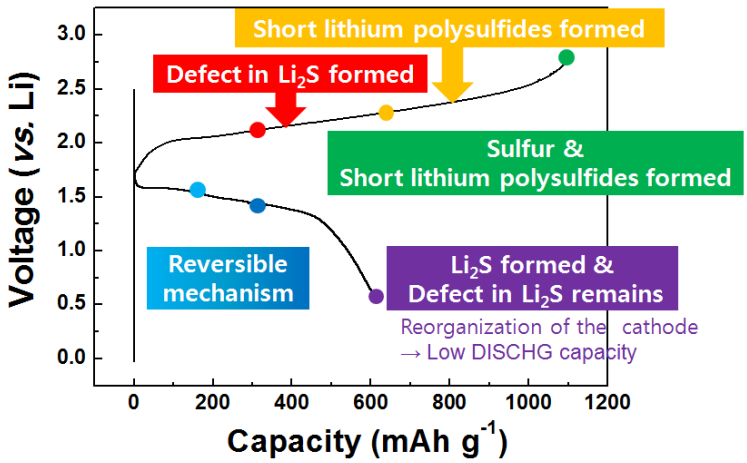

Fig. 4.11 Suggested all-solid-state Li-sulfur battery mechanism

Chapter 5. Conclusion

In this thesis, construction of all-solid-state Li-sulfur battery was carried out and stable charge/discharge was confirmed. To analyze mechanism on all-solid-state Li-sulfur battery, Raman spectroscopy and XPS was used, which can detect polysulfides as well as sulfur and Li_2S.

During charge, Li_2S was oxidized to defective Li_2S and later on to short-chain lithium polysulfide and finally to sulfur. During discharge, reverse reaction was occurred and defective Li_2S was remained after 1^{st} cycle. There was no evidence of long-chain lithium polysulfides in this experiment.

It is assumed that defective Li_2S and poor electrochemical performance are caused by reorganization of the cathode structure, which might be improved by controlling interfaces between cell components.

Bibliography

[1] J.-M. Tarascon and M. Armand(2001), “Issues and challenges facing rechargeable lithium batteries”, Nature, 414, pp. 359

[2] V. Etacheri, R. Marom, R. Elazari, G. Salitra and D. Aurbach(2011), “Challenges in the development of advanced Li-ion batteries: a review”, Energy Environ. Sci., 4, pp. 3243

[3] G. Jeong, Y.-U. Kim, H. Kim, Y.-J. Kim and J.-J. Sohn(2011), “Prospective materials and applications for Li secondary batteries”, Energy Environ. Sci., 4, pp. 1986

[4] M.-K. Song, E. J. Cairns, Y. Zhang(2013), “Lithium/sulfur batteries with high specific energy: old challenges and new opportunities”, Nanoscale, 5, pp. 2186

[5] J. Paris, and B. Plichon(1981), “ELECTROCHEMICAL REDUCTION OF SULPHUR IN DIMETHYLACETAMIDE”, Electrochem. Acta, 26 (12), pp. 1823

[6] H. Yamin, A. Gorenshtein, J. Penciner, Y. Sternberg, and E. Peled(1988), “Lithium Sulfur Battery Oxidation/Reduction Mechanisms of Polysulfdies in THF Solutions”, J. Electrochem. Soc., pp. 1045

[7] E. Peled, A. Gorenshtein, M. Segal, and Y. Sternberg(1989), “RECHARGEABLE LITHIUM-SULFUR BATTERY(EXTENDED ABSTRACT)” J. Power Sources, 26, pp. 269

[8] A. Manthiram, Y. Fu, and Y.-S. Su(2013), “Challenges and Prospects of

Lithium-Sulfur Batteries", Acc. Chem. Res., 46 (5), pp. 1125

[9] G. Eichinger, and J. Besenhard(1976), "HIGH ENERGY DENSITY LITHIUM CELLS PART II. CATHODES AND COMPLETE CELLS", J. Electroanal. Chem., 72, pp.1

[10] S.-E. Cheon, K.-S. Ko, J.-H. Cho, S.-W. Kim, E.-Y. Chin, and H.-T. Kim(2003), "Rechargeable Lithium Sulfur Battery I. Structural Change of Sulfur Cathode Durifng Discharge and Charge", J. Electrochem. Soc., 150 (6), pp. A 796

[11] Y.-J. Choi, Y.-D. Chung, C.-Y. Baek, K.-W. Kim, and H.-J. Ahn, J.-H. Ahn(2008), "discharge process of Li/PVdF/S cells at room temperature", J. Power Sources, 184, pp. 548

[12] S. S. Jeong, Y. T. Lin, Y. T. choi, G. B. Cho, K. W. Kim, H. J. Ahn, K. K. Cho(2007), "Electrochemical properties of lithium sulfur cells using PEO polymer electrolytes prepared under three different mixing conditions", J. Power Sources, 174 (2), pp. 745

[13] J. Nelson, S. Misra, Y. Yang, A. Jackson, Y. Liu, H. Wang, H. Dai, J. C. Andrews, Y. Cui, and M. F. Toney(2012), "In Operando X-ray Diffraction and Transmission X-ray Microscopy of Lithium Sulfur Batteries", J. Am. Chem. Soc., 134 (14), pp. 6377

[14] S. Walus, C. Barchasz, J.-F. Colin, J.-F. Martin, E. Elkaim, J.-C. Lepretre, and F. Alloin(2013), "New insight into working mechanism of Lithium/Sulfur batteries: in situ and operand X-ray diffraction characterization", Chem. Commun., 49, pp. 7899

[15] R. D. ARauh, F. S. Shuker, J. M. Marston, and S. Brummer(1977),

“FROMATION OF LITHIUM POLYSULFIDES IN APROTIC MEDIA”, J. Inorg. Nucl. Chem., 39, pp. 1761

[16] K. Kumareasan, Y. Mikhaylik, and R. E. White(2008), “A Mathmatical Model for a Lithium-Sulfur Cell”, J. Electrochem. Soc., 155 (8), pp. A 576

[17] C. Barchasz, F. Molton, C. Duboc, J.-C. Lepretre, S. Patoux, and F. Alloin(2012), “Lithium/Sulfur Cell Discharge mechanism: An Original Approach for Intermediate Species Identification”, Anal. Chem., 84, pp. 3973

[18] J.-T. Yeon, J.-Y. Jang, J.-G. Han, J. Cho, K. T. Lee, and N.-S. Choi(2012), “Raman Spectroscopic and X-ray Diffraction Studies of Sulfur composite Electrodes during Discharge and Charge”, J. Electrochem. Soc., 159 (8), pp. A 1308

[19] Y. Yang, G. Zheng, and Y. Cui(2013), “A membrane-free lithium/polysulfide semi-liquid battery for large-scale energy storage”, Energy Environ. Sci., 6, 1552

[20] Y. V. Mikhaylik, and J. R. Akridge(2003), “Low Temperature Performance of Li/S batteries”, J. Electrochem. Soc., 150 (3), pp. A 306

[21] L. Suo, Y.-S. Hu, H. Li, M. Armand, and L. Chem, “A new class of Solvent-in-Salt electrolyte for high-energy rechargeable metallic lithium batteries”, Nature Commun.,

[22] R. Elazari, G. Salitra, Y. Talyosef, J. Grinblat, C. S.-Kelley, A. Xiao, J. Affinito, and D. Aurbach,(2010), “Morphological and Structural Studies of Composite Sulfur Electrodes upon Cycling by HRTEM, AFM, and Raman Spectroscopy”, J. Electrochem. Soc., 157 (10), pp. A 1131

[23] X. Ji, K. T .Lee, and L. F. Nazar(2009), “A highly ordered nanostructured

carbon-sulphur cathode for lithium-sulphur batteries", Nature Mat., 8, pp. 500

[24] S. Xin, L. Gu, N.-H. Zhao, Y.-X. Yin, L.-J. Zhou, Y.-G. Guo, and L.-J. Wan(2012), "Smaller Sulfur Molecules Promise Better Lithium-Sulfur batteries", J. Am. Chem. Soc., 134 (45), pp. 18510

[25] G. Zheng, Q. Zhang, J. J. Cha, Y. yang, W. Li, Z. W. She, and Y. Cui(2012), "Amphiphilic Surface Modification of Hollow Carbon Nanofibers for Improved Cycle Life of Lithium Sulfur Batteries", Nano. Lett., 13 (3), pp. 1265

[26] J. Wang, J. Yang, C. Wan, K. Du, J. Xie, and N. Xu(2003), "Sulfur Composite Cathode materials for Rechareable Lithium Batteries", Adv. Funct. Mater., 13, pp. 487

[27] J. Guo, Z. Yang, Y. Yu, H. D. Abruna, and L. A. Archer(2013), "Lithium-Sulfur Battery Cathode Enabled by Lithium-Nitrile Interaction", J. Am. Chem. Soc., 135, pp. 763

[28] W. Li, G. Zheng, Y. Yang, Z. W. She, N. Liu, and Y. Cui(2013), "High-performance hollow sulfur nanostructured battery cathode through a scalable, room temperature, one-step, bottom-up approach", PANS, 110 (18), 7148

[29] Z. W. She, W. Li, J. J. Cha, G. Zheng, Y. Yang, M. T. McDowell, P-C. Hsu, and Y. Cui(2012), "Sulphur-TiO2 yolk-shell nanoarchitecture with internal void space for long-cycle lithium-sulphur batteries", Nature Commun., 4 (1331), pp. 1

[30] B. Ding, L. Shen, G. Xu, P. Nie, and X. Zhang(2013), "Encapsulating sulfur into mesoporous TiO_2 host as a high performance cathode for lithium-sulfur battery", Electrochimica Acta, 107, pp. 78

[31] C.-S. Kim, A. Guerfi, P. Hovington, J. Trottier, C. Gagnon, F. Barray, A. vijh, M. Armand, and K. Zaghib(2013), “Facile dry synthesis of sulfur-$LiFePO_4$ core-shell composite for the scalable fabrication of lithium/sulfur batteries”, Electrochem. Commun., 32, pp. 35

[32] L. Wang, D. Wang, F. Zhang, and J. Jin(2013), “Interface Chemistry Guided Long-Cycle-Life Li-S battery”, Nano Lett., 13 (9), 4206

[33] Y. Yang, G. Zheng, and Y. Cui(2013), “A membrane-free lithium/polysulfide semi-liquid battery for large-scale energy storage”, Energy Environ Sci., 6, 1552

[34] R. D.-Cakan, m. Morcrette, Gangulibabu, A. Gueguen, R. Dedryvere, and J.-M. Tarascon(2012), “Li-S batteries: simple approaches for superior performance”, Energy Environ. Sci., 6, pp. 176

[35] Y. Fu, Y.-S. Su, and A. Manthiram(2013), “Highly Reversible Lithium/Dissolved Polysulfdie Batteries with Carbon Nanotube Electrodes”, Angew. Chem. Int. Ed., 52, pp. 1

[36] S. S. Zhang(2012), “Role of LiNO3 in rechargeable lithium/sulfur battery”, Electrochemica Acta, 70, pp. 344

[37] Z. Lin, Z. Liu, W. Fu, N. J. Dudney, and C. Liang, “Phosphorous Pentasulfide as a Novel Additive for High-performance Lithium-Sulfur Batteries”, Adv. Funct. Mater., pp. 1

[38] Y.-S. Su, and A. Marthiram(2012), “Lithium-sulphur batteries with a microporous carbon paper as a bifunctional interlayer”, Naterure Commun., 3

[39] D.-R. Chang, S.-H. Lee, S.-W. Kim, and H.-T. Kim(2002), “Binary electrolyte based on tetra(ethylene glycol) dimethyl ether and 1,3-dioxolane

for lithium-sulfur battery", J. Power Sources, 112, pp. 452

[40] H. S. Kim, and C.-S. Jeong(2012), "Shuttle inhibitor effect of lithium perchlorate as an electrolyte salt for lithium-sulfur batteries", J. Appl. Electrochem., 42, pp. 75

[41] J. Gao, M. A. Lowe, Y. Kiya, and H. D. Abruna(2011), "Effects of Liquid Electrolytes on the Charge-Discharge Performance of Rechargeable Lithium/Sulfur Batteries: Electrochemical and in-Situ X-ray Absorption Specctroscopic Studies", J. Phys. Chem. C, 115, pp. 25132

[42] M. Nagao, A. Hayashi, and M. Tatsumisago(2011), "Sulfur-carbon composite electrode for all-solid-state Li/S battery with Li_2S-P_2S_5 solid electrolyte", Electrochimica Acta, 56, pp. 6055

[43] M. Nagao, A. Hayashi, and M. Tatsumisago(2012), "High-capacity Li_2S-nanocarbon composite electrode for all-solid-state rechargeable lithium batteries", J. Mater. Chem., 22, pp. 10015

[44] M. Nagao, A. Hayashi, and M. Tatsumisago(2012), "Fabrication of favorable interface between sulfide solid electrolyte and Li metal electrode for bulk-type solid-state Li/S battery", Electrochem. Commun., 22, pp. 177

[45] Z. Lin, Z. Liu, N. J. Dudney, and c. Liang(2013), "Lithium Superionic Sulfide Cathode for All-solid-Lithium-Sulfur Batteries", ACS Nano,

[46] M. Murayama, n. Sonoyama, A. Yamada, and R. kanno(2004), "Materials design of news lithium ionic conductor, thio-LiSICON, in the Li_2S-P_2S_5 system", Solid State Ionics, 170, pp. 173

[47] M. Murayama, R. Kanno, Y. Kawamoto, and T. Kamiyama(2002), "structure of the thio-LiSICON, Li_4GeS_4", Solid State Ionics, 154-155, pp.

789

[48] A. Hayashi, S. Hama, T. Minami, and M. Tatsumisago(2003), “Formation of superionic crystals from mechanically milled Li_2S-P_2S_5 glasses”, Electrochem. Commun., 5, pp. 111

[49] T. Takeuchi, H. Kageyama, K. Nakanishi, M. Tabuchi, H. Sakaebe, T. Ohta, H. Senoh, T. Sakai, and K. Tatsumi(2010), “All-Solid-State Lithium Secondary Battery with Li_2S-C Composite Positive Electrode Prepared by Spark-Plasm-Sintering Process”, J. Electrochem. Soc., 157 (11), pp. A 1196

[50] A. Sakuda, A. Hayashi, and M. Tatsumisago(2013), “Sulfide Solid Electrolyte with Favorable Mechanical Property for All-Solid-State Lithium Battery”, Scientific Reports, 3, pp. 1

[51] M. Hiratani, K. Miyauchi, and T. Kudo(1988), “EFFECT OF A LITHIUM ALLOY LAYER INSERTED BETWEEN A LITHIUM ANODE AND A SOLID ELECTROLYTE”, Solid State Ionics, 28-30, pp. 1406

[52] Y. Yangt, G. Zheng, S. Misra, J. Nelson, M. F. Toney, and Y. Cui(2012), “High-Capacity Micrometer-Sized Li_2S Particles as Cathode Materials for Advanced Rechargeable Lithium-Ion Batteries”, J. Am. Chem. Soc., 134(37), pp. 15387

[53] Y. Diao, K. Xie, S. Xiong, and X. Hong(2013), “Shuttle phenomenon – The irreversible oxidation mechanism of sulfur active materials in Li-S battery”, J. Power Sources, 235, pp. 181

국 문 요 약

최근 들어 용량이 크고, 저렴하며 자연친화적인 황으로 리튬 이온 전지를 구상하려는 연구가 각광받고 있다. 하지만, 리튬 폴리설파이드(중간 방전 생성물)가 액체 전해질에 용해되어 부반응(shuttle mechanism)을 함으로써 (방전 용량 저하, 과충전) 수명특성을 저하시키는 문제가 발생하고 있다. 따라서 본 연구에서는 부반응을 제거한 고체전해질을 리튬 황 전지에 적용하고 메커니즘을 분석하고자 한다. 이에 간단한 저온 공정으로도 높은 이온 전도도를 가지며, 금속 음극과 안정한 반응을 할 수 있는 Li_2S-P_2S_5 황화물계 리시콘 II 유사체를 고체전해질로 선정하였다. 그리고 표준화가 이루어진 액체 전해질 시스템과 다른 전 고체 리튬 황 전지 시스템을 구축하여 성능을 평가하였다. 중간생성물과 반응 메커니즘을 확인하기 위하여 Raman spectroscopy와 X-ray photoelectron spectroscopy를 사용하였다. 그 결과 충전과정 중에는 Li_2S가 결함있는 Li_2S를 형성한 후 짧은 리튬 폴리설파이드를 거쳐서 황을 형성했다. 방전과정 중에는 그 역 반응이 일어났다. 첫 번째 방전과정 후 남아있는 defective Li_2S이 비가역 용량과 수명 특성 저하의 원인으로 예측되며 탄소-황- 고체전해질 복합체가 특성 개선에 도움이 될 것이다

주요어: 전 고체, 리튬 황 전지, 황화물계 리시콘, 결함있는 Li_2S, 폴리설파이드
학 번: 2012-20583